Temperature dependence of stacking faults in catalyst-free GaAs nanopillars

Temperature dependence of stacking faults in catalyst-free GaAs nanopillars

Joshua N Shapiro[1]**, Andrew Lin**[1]**, Christian Ratsch**[2] **and D L Huffaker**[1]

[1] UCLA Electrical Engineering and California Nano-Systems Institute, USA
[2] UCLA Mathematics and Institute for Pure and Applied Math, USA

E-mail: joshua.shapiro@gmail.com

Abstract

Impressive opto-electronic devices and transistors have recently been fabricated from GaAs nanopillars grown by catalyst-free selective-area epitaxy, but this growth technique has always resulted in high densities of stacking faults. A stacking fault occurs when atoms on the growing (111) surface occupy the sites of a hexagonal-close-pack (hcp) lattice instead of the normal face-centered-cubic (fcc) lattice sites. When stacking faults occur consecutively, the crystal structure is locally wurtzite instead of zinc-blende, and the resulting band offsets are known to negatively impact device performance. Here we present experimental and theoretical evidence that indicate stacking fault formation is related to the size of the critical nucleus, which is temperature dependent. The difference in energy between the hcp and fcc orientation of small nuclei is computed using density-function theory. The minimum energy difference of 0.22 eV is calculated for a nucleus with 21 atoms, so the population of nuclei in the hcp orientation is expected to decrease as the nucleus grows larger. The experiment shows that stacking fault occurrence is dramatically reduced from 22% to 3% by raising the growth temperature from 730 to 790 °C. These data are interpreted using classical nucleation theory which dictates a larger critical nucleus at higher growth temperature.

(Some figures may appear in colour only in the online journal)

Nanopillars grown by catalyst-free selective-area epitaxy (CF-SAE) have recently been used as the platform for an impressive array of electronic devices including nano-lasers, photo-voltaics, avalanche photo-diodes, and high speed transistors [1–4]. Despite these successes, stacking faults, or rotational twins, are a common defect whose presence is accountable for phenomena such as reduced mobility, carrier localization, and increased resistivity [5–8]. These effects are caused by scattering at the twin planes, and by the modified band structure in regions with consecutive stacking faults where the crystal structure is wurtzite (WZ) instead of zinc-blende (ZB). This polytypism is also an impediment to the realization of nanopillar based inter-subband devices that will require exquisite control of the band structure. For these reasons, control of stacking faults and polytypism in nanowires has been a major focus of research, and has been met with considerable success for Au catalyzed nanowires [9–12, 12–16].

This paper focuses on the cause and reduction of stacking faults in nanopillars grown by CF-SAE. This growth mode is different from the more common Au catalyzed vapor–liquid–solid (VLS) nanowire epitaxy. In CF-SAE, a thin dielectric mask is deposited on a substrate (GaAs 111B for this work), then the mask is patterned with an array of nano-holes by electron beam lithography and reactive-ion etching, and the nanopillars are grown by metal-organic chemical vapor deposition [17–19]. GaAs nanopillars grow vertically to lengths of several microns, with minimal increase in diameter, at temperatures above 700 °C in the patterned holes. Figure 1 shows scanning electron microscope (SEM) images of a SiO$_2$ coated GaAs substrate patterned with an array of nano-holes, and the resulting nanopillar array after growth. Stacking faults are common for both growth methods, but several papers have demonstrated control of stacking fault formation in Au catalyzed epitaxy, whereas no control of stacking faults has been demonstrated in CF-SAE nanopillars until now.

In this paper we show that stacking fault formation is dramatically reduced by raising the growth temperature, and explain this experimental result with total energy
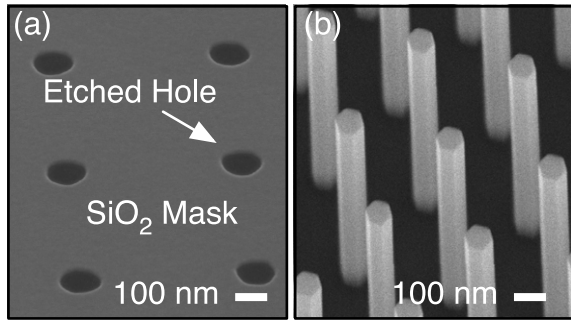
1

Figure 1. (a) SEM image of a GaAs substrate coated with a 20 nm SiO$_2$ film that has an array of nano-holes patterned by electron beam lithography and reactive-ion etching. (b) Tilted SEM image of the nanopillar array. Each nanopillar grows from an etched nano-hole.

calculations of small nuclei on the GaAs (111)B using density-functional theory (DFT). Figure 2 shows transmission electron microscope (TEM) images from 140 nm diameter GaAs nanopillars grown at 730 and 790 °C, and from a 220 nm diameter nanopillar grown at 790 °C. The samples were all grown for 12 min by metal-organic chemical vapor deposition in a hydrogen environment at 60 Torr with tri-methyl-gallium and tertiary-butyl-arsine precursors at molar flow rates of 1.01×10^{-5} and 9.8×10^{-5} mol min^{-1} respectively. Stacking faults are indicated by black arrows. The number of stacking faults is noticeably reduced for the samples grown at higher temperature.

Figure 2 also shows histograms of the distance between stacking faults measured from the shown TEM, and from TEM images of two other nanopillars from each sample. For the sample grown at 730 °C, 69 stacking faults are counted over a total of 388 bi-layers corresponding to a stacking fault density $N_{\text{hcp}}/N_{\text{fcc}} = 22\%$. In contrast, the 140 nm diameter nanopillars grown at 790 °C have 19 stacking faults over 286 bi-layers for a density $N_{\text{hcp}}/N_{\text{fcc}} = 7\%$, and the 220 nm diameter nanopillars grown at 790 °C have only 13 stacking faults over 434 bi-layers, for a stacking fault density $N_{\text{hcp}}/N_{\text{fcc}} = 3\%$. The nanopillars grown at 790 °C have a noticeable reduction in stacking faults, and these data also indicate a mild diameter dependence, with larger diameters having fewer stacking faults. No data were collected for large diameter nanopillars grown at 730 °C, but Yoshida *et al* measured the total proportion of WZ segments to be 15.6% in a 200 nm diameter nanopillar [20].

These data show a quantifiable decrease in the density of stacking faults simply by raising the growth temperature, and a mild diameter dependence with the stacking fault density decreasing for larger diameter. A similar trend of decreased stacking faults with increasing temperature has been inferred in other work by examining the orientation of tetrahedrons that grow in large diameter selective-area mask openings, but no direct evidence has been presented nor has an explanation been proposed [19, 20]. We hypothesize that the temperature dependence is due to an increase in the size of the critical nucleus at higher temperature. This theory will be addressed
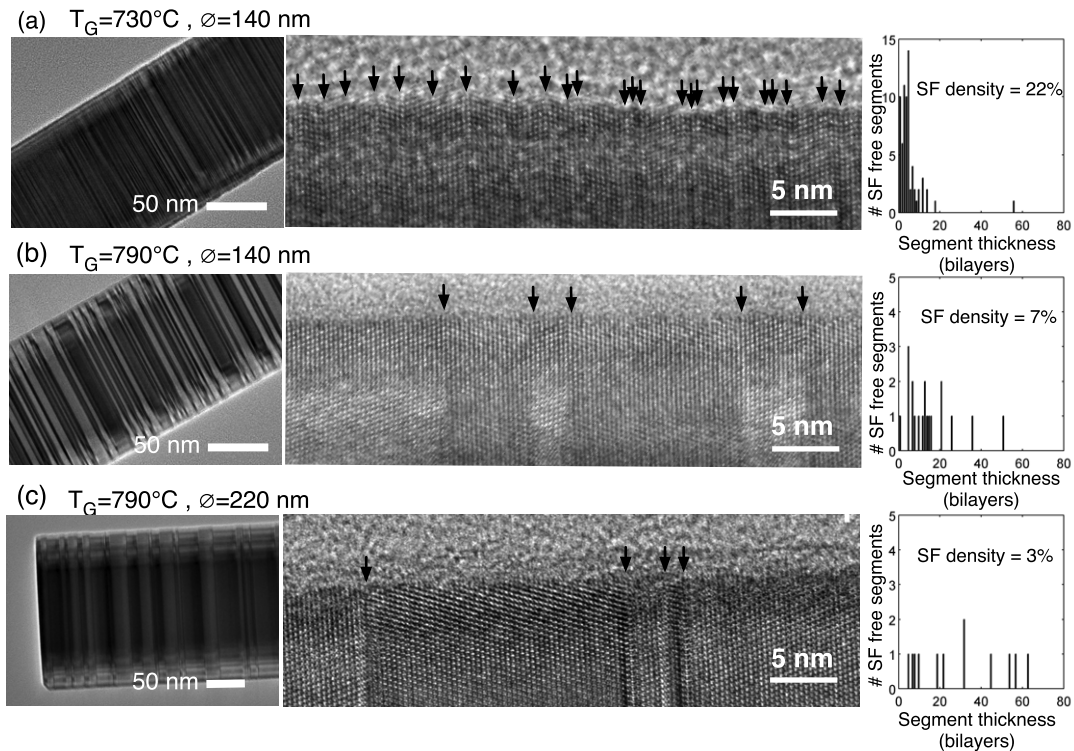

Figure 2. Low and high resolution TEM and histograms of the number of stacking fault (SF) free segments versus the segment thickness in bi-layers for (a) 140 nm diameter GaAs nanopillar grown at 730 °C, (b) 140 nm diameter grown at 790 °C, and (c) 220 nm diameter grown at 790 °C.

in depth in this paper. We speculate the increase in stacking fault density for smaller diameters is related to a faster vertical growth rate, which translates to a faster nucleation rate. When the nucleation rate is fast, a nucleus in the hcp orientation can grow into a stable island before shifting into the more energetically favorable fcc orientation.

The theory of stacking fault formation is well developed for the VLS growth mode, but poorly understood in catalyst-free epitaxy. Stacking fault formation in Au catalyzed nanowires is driven by nucleation, which occurs at the triple-phase line where the nanowire, the liquid catalyst, and the vapor meet. Nucleation in the fcc or hcp orientation is governed by the free energy of the nucleus, and the surface energies of the droplet and the exposed semiconductor. The free energy depends on the super-saturation of the droplet, and works in conjunction with the energy gain from 'eliminating a portion of the pre-existing droplet surface' [21, 22]. The super-saturation and geometry of the droplet depend on diameter, temperature, and V/III ratio [14, 15]. The diameter dependence of stacking faults is attributed to the Gibbs–Thomson effect which increases the super-saturation in smaller diameter droplets, thereby increasing the occurrence of WZ in the nanowire [14]. The surface energy of the crystal changes as the surface reconstructs for different V/III ratios. This effects the geometry of the facets and the shape of the droplet at the liquid–vapor–solid interface where nucleation occurs [10, 15]. Control of crystal phase in self-catalyzed GaAs nanowires grown with a Ga droplet on top have also been demonstrated [5, 23]. The explanation for this phenomena in the self-catalyzed mode again hinges on the precise location of nucleation as determined by the shape and contact angle of the droplet with the crystalline semiconductor. The droplet, in turn, is controlled by V/III ratio in the case of self-catalyzed nanowires [24]. Because the ability to control the crystal phase in VLS growth depends intimately on the liquid droplet, these results are not directly applicable to CF-SAE nanopillars. However in VLS growth, the theory is ultimately based on which nucleus, hcp or fcc, lowers the free energy of the system the most.

Prior attempts to explain stacking fault formation in CF-SAE nanopillars invoke the lower surface energy of a WZ crystal and the contributions of surfaces and edges to the formation energy [25–28]. They attribute the stabilization of WZ to the energetic penalty of additional dangling bonds at the edges of a ZB nanopillar, where the corner atoms are only two-fold coordinated. Models based on these calculations predict the diameter of transition from WZ to ZB to be 5–10 nm, but dense stacking faults are routinely observed in nanopillars hundreds of nanometers in diameter and even in thin films. While the role of the side facets can dominate at very small diameters, the prevalence of stacking faults at large diameters and in planar epitaxy on (111)B indicates a non-equilibrium process intimately related to the (111)B surface is the driving force behind stacking fault formation.

Because there is no droplet in CF-SAE, the growth mode is similar to traditional planar epitaxy on the (111)B surface, which is governed by nucleation and island growth. Studies of thin film epitaxy on GaAs (111)B show that both the surface roughness and the density of stacking faults are related to the GaAs (111)B surface reconstruction [29–34]. In brief, stacking faults are abundant and the surface is rough when growth is initiated at lower temperatures on the (2×2) As trimer and $(1 \times 1)_{LT}$ surface reconstruction. Fewer stacking faults and a smooth surface form at higher temperature when the growth is initiated on the $(\sqrt{19} \times \sqrt{19})R23.4°$ and $(1 \times 1)_{HT}$ surfaces. The general conclusion from these thin film growth experiments is that stacking fault formation is intimately linked to the (111)B surface and not a byproduct of surface or edge energies from other surfaces.

To understand the reason that higher growth temperature reduces stacking fault density, we mirror the VLS theory of stacking fault formation which compares the Gibbs free energy of a normal (fcc) and a twin-plane (hcp) nucleus. Here we compare the total energy of several small nuclei in the normal fcc orientation and the twinned hcp orientation on an unreconstructed GaAs (111)B surface. Assuming a critical nucleus can form in the hcp orientation, then as the nucleus aggregates adatoms and an island forms, the stacking fault becomes frozen into the crystal. At higher growth temperatures, the critical nucleus is larger because the rate at which islands de-aggregate is high [35]. The stacking fault probability is given by $\exp(-\Delta E/k_B T)$, where $\Delta E = E_{hcp} - E_{fcc}$ is the difference in energy between the two types of nuclei [13–15]. Our calculations show that the energy difference between an fcc and hcp oriented nucleus depends on the size of the nucleus. The fcc orientation has lower energy for all the nuclei, so ΔE is always positive. fcc is strongly favored for the smallest nucleus, but ΔE decreases, reaches a minimum, then increases as the nucleus grows. Stacking faults will be prevalent at the minimum of ΔE, but will decrease with temperature as the size of the critical nucleus grows and ΔE increases.

Ground state energies are calculated using DFT as implemented in the FHI-AIMS code [36], which uses numeric atom-centered orbitals for its basis set and includes a zero-order relativistic correction for heavy atoms (atomic number > 30). The Perdew–Burke–Ernzerhof (PBE) [37] functional is used with the pre-defined AIMS 'light' settings, where every atom has radial basis functions of s, p, and d like character, an overall cutoff radius of 5 Å, and a local Hartree potential expansion up to $l = 4$. Selected results were checked with the 'tight' settings which have a finer integration grid, an additional f like basis function, an overall cutoff radius of 6 Å, and a local Hartree potential expansion up to $l = 6$. Energy differences computed with the 'tight' settings differed from the 'light' settings by less than 10 meV, so the 'light' settings are used for the remainder of the calculations.

Five different nuclei are compared in the fcc and hcp orientations on the unreconstructed (111)B surface. Three of the nuclei are also computed in an intermediate hybrid (HYB) orientation. The three orientations are pictured for the largest nucleus, a 22-atom triangular nucleus (12 Ga + 10 As), in figure 3. There is a 60° angle between the fcc and hcp orientations. The HYB orientation is rotated 30° from both the hcp and fcc orientations, and the nucleus is displaced
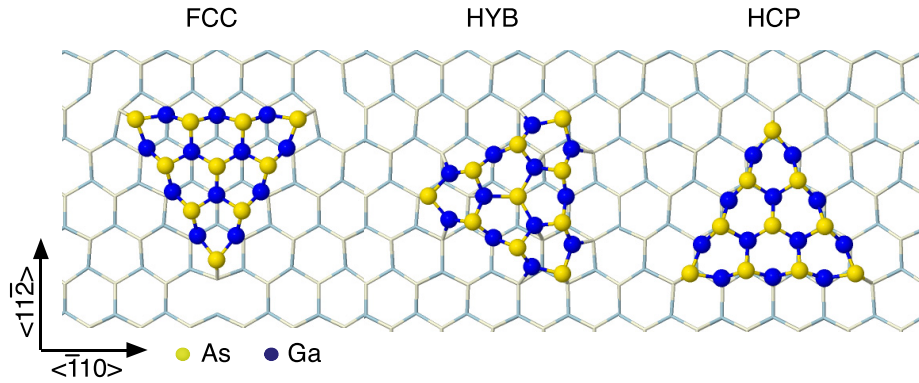
Figure 3. A 22 atom (12 Ga + 10 As) nucleus on a (111)B slab in the fcc, HYB, and hcp orientations. This nucleus in the HYB orientation appears in the ($\sqrt{19} \times \sqrt{19}$)R23.4° reconstruction.

so that the central As atom is directly above and bonded to an As atom in the slab. In the HYB orientation, the pictured nucleus has 16 bonds with the slab, whereas in the fcc and hcp orientations, there are only 15 bonds between the nucleus and the slab. The HYB orientation is stable, and in fact has lower energy than either of the other orientations for the tested nuclei, but none of the atoms sit in conventional lattice sites. For the layer to complete and from a fcc or hcp crystal, a nucleus in the HYB orientation must transition to either the fcc or hcp orientation.

The remaining nuclei are pictured in figure 4 along with the total energy difference between the hcp and fcc orientation. The smallest and largest nuclei are based on structures observed in experimental studies. The intermediate nuclei are speculative, but realistic based on our knowledge of atom arrangements and bond angles for GaAs. The smallest nuclei has 1 Ga and 3 As atoms, and is based on a four atom structure observed in STM maps of the $(1 \times 1)_{LT}$ transition region [33]. The next smallest is a compact hexagon with 3 Ga and 3 As atoms. No direct observation of the (3 Ga + 3 As) nucleus exists on GaAs (111)B, but compact six atom hexagonal nuclei have been observed on InSb (111)B surfaces [38]. The triangular (7 Ga + 6 As) nucleus has also not been observed experimentally, but it is a natural candidate given the symmetry of the surface and the experimental evidence for the largest nuclei. The largest nuclei calculated are the (12 Ga + 9 As) and (12 Ga + 10 As), which in the HYB orientation are the 'unfilled' and 'filled' atomic configurations of the ($\sqrt{19} \times \sqrt{19}$)R23.4° reconstruction commonly observed in STM and recently computed by Koga [29, 30, 39, 40].

The total energy of each nucleus is calculated using 6×6 and 7×7 super-cells that are 5 bi-layers thick with 30 Å of vacuum separating the periodic slab images in the z-direction. The bottom surface of the slab is terminated with fractional hydrogen atoms. The nucleus and the top four layers of the slab are allowed to relax until residual forces on each atom are less than 0.020 eV Å^{-1}. The energies are converged for slab thickness and k-points, and we estimate that the numbers are converged to within 0.1 eV with respect to super-cell size.

The total energy difference between the hcp and fcc orientations for each nuclei is plotted in figure 4. The dashed,
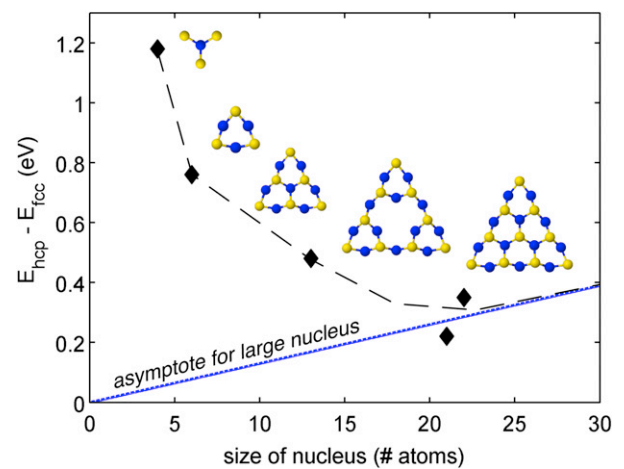

Figure 4. The energy difference (black diamonds) between fcc and hcp orientation of computed nuclei. Each calculated nucleus is shown in order of increasing size. The blue line is the energy difference for a complete bi-layer of hcp on a fcc slab. The dashed black line is a guide for the eye.

blue line is the stacking fault energy of 0.026 eV per GaAs pair, that is calculated by taking the difference in total energy between two 1×1 slabs 10 bi-layers thick. One slab has pure fcc stacking and the top layer of the second slab is oriented in the hcp arrangement. Moving from smallest to largest, the nuclei favor the fcc orientation by 1.18 eV, 0.75 eV, 0.48 eV, 0.22 eV and 0.35 eV respectively, and converge to the stacking fault energy asymptotically. We believe the energy difference has reached a minimum for the calculated 21 and 22 atom nuclei, and will increase along the asymptote for even larger nuclei.

To understand the experimental evidence in terms of this computed trend, recall that in classical nucleation theory the size of the critical nucleus is larger at higher temperature. In temperature regimes where stacking faults are prevalent, we hypothesize that the critical nucleus is similar in size to the (12 Ga + 9 As) nucleus. With a calculated energy difference of $\Delta E = 0.22$ eV and a growth temperature of $T_G = 730\,°C$ ($k_B T = 0.086$ eV), the expected stacking fault density is 8%. Projecting along the asymptote to larger nuclei, the next
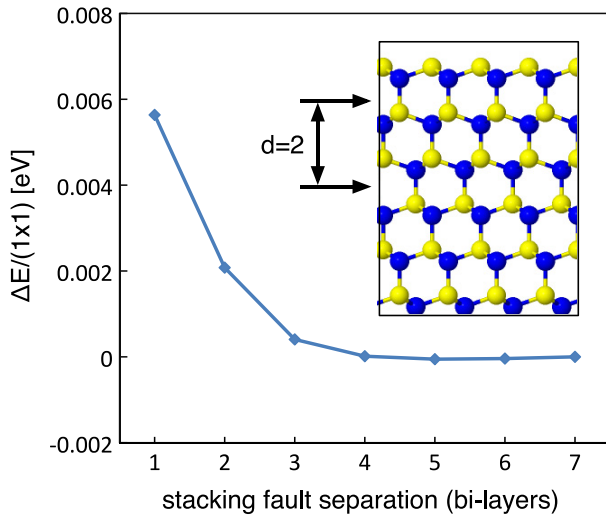
Figure 5. The difference in total energy between slabs with two stacking faults separated by a distance *d*. Inset shows the top 6 bi-layers of a slab with a stacking fault separation of $d = 2$. The zero-point energy is arbitrarily defined as the energy difference when $d = 7$.

Table 1. The relative energy between the HYB orientation and the fcc and hcp orientations for three nuclei.

Nucleus	$E_{fcc} - E_{hyb}$ (eV)	$E_{hcp} - E_{hyb}$ (eV)
(3 Ga + 3 As)	1.80	2.55
(12 Ga + 9 As)	2.59	2.81
(12 Ga + 10 As)	3.39	3.74

difference for three of the nuclei are presented in table 1. A nucleus in the HYB orientation has lower energy than either of the other two orientations by a minimum of 1.8 eV. One possible reason for this drastic difference is because a nucleus in the HYB orientation can fill more of the surface As dangling bonds than the other two orientations. This is evident for the (12 Ga + 10 As) HYB nucleus by directly counting the atoms bonded to the slab surface. However, the (12 Ga + 9 As) HYB and the (3 Ga + 3 As) HYB nucleus have the same number of bonds between the nucleus and the surface as in the fcc and hcp orientations. A rudimentary electron counting analysis for these nuclei suggests that electrons from the nucleus are available to fill this exposed dangling bond in the central As atom which will lower the energy [41].

It is interesting to note that Yoshida *et al* estimate the activation energy for stacking fault elimination at $E_A = 3.7$ eV, but they do not speculate on the meaning of this activation energy [20]. One possible avenue for layer completion is for HYB nuclei to flip into either the hcp or fcc orientation and then aggregate atoms to become stable and grow. The energy barriers and transition pathway from the HYB orientation to hcp or fcc is unknown, but we note that the energy differences calculated for the (12 Ga + 10 As) nucleus are in rough agreement with the activation energy measured by Yoshida.

In conclusion, we have shown that stacking faults can be dramatically reduced in nanopillars grown by CF-SAE at a growth temperature of 790 °C. The total energy of five different nuclei ranging in size from 4 to 22 atoms are computed in the fcc, hcp, and in a HYB orientation on the (111)B. The difference in energy between hcp and fcc has a minimum for nuclei with approximately 21 atoms, so the reduction in stacking fault density at higher temperature can be explained if the critical nucleus is 21 atoms at a growth temperature of 730 °C, and larger for higher temperature. We show that there is an energetic penalty when stacking faults are closer than 4 bi-layers. Finally, we note that the HYB nucleus has the lowest energy of the three configurations by an amount that is in rough agreement with the activation energy previously measured to eliminate stacking faults. This may indicate that the transition path on the potential energy landscape includes a crossing through a HYB oriented nucleus.

largest triangular nucleus has 18 Ga and 15 As atoms. With 33 atoms the energy difference between the two orientations of this nucleus is 0.43 eV ($\Delta E = 33 \times -0.026 \div 2$), and the corresponding stacking fault density at a $T_G = 790$ °C ($k_B T = 0.092$ eV) is 1%. The absolute numbers for stacking fault density are not in exact agreement with the experiment, but the reduction in stacking fault density has the same order of magnitude for experimental measurements and theoretical calculations. This analysis also agrees with studies of planar epitaxy on GaAs (111)B that report a reduction in stacking faults for growth on the $(\sqrt{19} \times \sqrt{19})$R23.4° reconstruction. This surface is tiled with (12 Ga + 9 As) HYB nuclei which must be below the size of the critical nucleus because they fail to grow into islands.

We also investigate the effect of multiple stacking faults in a slab, and examine the stacking fault energy as the distance between stacking faults increases. To study this, we calculate the difference in total energy between slabs of GaAs (111)B containing two stacking faults. One stacking fault is fixed at the top of the slab, and the second is incrementally moved deeper into the slab. Each unreconstructed slab is 14 bi-layers thick, has a (1 × 1) unit cell and 30 Å of vacuum. The bottom 3 bi-layers are constrained in the bulk position while the top 11 bi-layers are allowed to relax. The difference in total energy for as a function of stacking fault separation is shown in figure 5, using the total energy of the slab with a stacking fault separation $d = 7$ as the energy zero point. The inset illustrates a stacking fault separation of 2 bi-layers. These data show an energy penalty when stacking faults are closer than 4 bi-layers. This calculation indicates that stacking faults directly below the (111)B surface may raise the energy of the hcp nucleus relative to the fcc nucleus and suppress the formation of adjacent stacking faults.

Now we will address the energy difference between the HYB orientation and the fcc/hcp orientations. The energy

Acknowledgments

References

[1] Senanayake P, Hung C-H, Farrell A, Ramirez D A, Shapiro J, Li C-K, Wu Y-R, Hayat M M and Huffaker D L 2012 *Nano Lett.* **12** 6448–52

[2] Scofield A C, Kim S-H, Shapiro J N, Lin A, Liang B, Scherer A and Huffaker D L 2011 *Nano Lett.* **11** 5387–90

[3] Tomioka K, Yoshimura M and Fukui T 2012 *Nature* **488** 189–92

[4] Tanaka T, Tomioka K, Hara S, Motohisa J, Sano E and Fukui T 2010 *Appl. Phys. Express* **3** 025003

[5] Spirkoska D *et al* 2009 *Phys. Rev.* B **80** 245325

[6] Thelander C, Caroff P, Plissard S, Dey A W and Dick K A 2011 *Nano Lett.* **11** 2424–9

[7] Lin A, Shapiro J N, Senanayake P N, Scofield A C, Wong P-S, Liang B and Huffaker D L 2012 *Nanotechnology* **23** 105701

[8] Shimamura K, Yuan Z, Shimojo F and Nakano A 2013 *Appl. Phys. Lett.* **103** 022105

[9] Algra R E, Verheijen M A, Borgstrom M T, Feiner L-F, Immink G, van Enckevort W J P, Vlieg E and Bakkers E P A M 2008 *Nature* **456** 369–72

[10] Algra R E, Verheijen M A, Feiner L-F, Immink G G W, Enckevort W J, Vlieg E and Bakkers E P A M 2011 *Nano Lett.* **11** 1259–64

[11] Caroff P, Dick K A, Johansson J, Messing M E, Deppert K and Samuelson L 2009 *Nature Nanotechnol.* **4** 50–5

[12] Dick K A, Bolinsson J, Messing M E, Lehmann S, Johansson J and Caroff P 2011 *J. Vac. Sci. Technol.* B **29** 04D103

[13] Johansson J, Karlsson L S, Svensson C P T, Martensson T, Wacaser B A, Deppert K, Samuelson L and Seifert W 2006 *Nature Mater.* **5** 574

[14] Johansson J, Dick K A, Caroff P, Messing M E, Bolinsson J, Deppert K and Samuelson L 2010 *J. Phys. Chem.* C **114** 3837–42

[15] Joyce H J, Wong-Leung J, Gao Q, Tan H H and Jagadish C 2010 *Nano Lett.* **10** 908–15

[16] Johansson J, Karlsson L S, Dick K A, Bolinsson J, Wacaser B A, Deppert K and Samuelson L 2009 *Cryst. Growth Des.* **9** 766–73

[17] Motohisa J, Noborisaka J, Takeda J, Inari M and Fukui T 2004 *J. Cryst. Growth* **272** 180–5

[18] Noborisaka J, Motohisa J and Fukui T 2005 *Appl. Phys. Lett.* **86** 213102

[19] Ikejiri K, Sato T, Yoshida H, Hiruma K, Motohisa J, Hara S and Fukui T 2008 *Nanotechnology* **19** 265604

[20] Yoshida H, Ikejiri K, Sato T, Hara S, Hiruma K, Motohisa J and Fukui T 2009 *J. Cryst. Growth* **312** 52–7

[21] Glas F, Harmand J C and Patriarche G 2007 *Phys. Rev. Lett.* **99** 146101

[22] Dubrovskii V G and Sibirev N V 2009 *Tech. Phys. Lett.* **35** 380–3

[23] Krogstrup P, Popovitz-Biro R, Johnson E, Madsen M H, Nygard J and Shtrikman H 2010 *Nano Lett.* **10** 4475–82

[24] Krogstrup P, Curiotto S, Johnson E, Aagesen M, Nygard J and Chatain D 2011 *Phys. Rev. Lett.* **106** 125505

[25] Akiyama T, Sano K, Nakamura K and Ito T 2006 *Japan. J. Appl. Phys.* **45** L275–8

[26] Akiyama T, Nakamura K and Ito T 2006 *Phys. Rev.* B **73** 235308

[27] Pankoke V, Kratzer P and Sakong S 2011 *Phys. Rev.* B **84** 075455

[28] Leitsmann R and Bechstedt F 2007 *J. Appl. Phys.* **102** 063528

[29] Avery A R, Tok E S and Jones T S 1997 *Surf. Sci.* **376** L397–402

[30] Chen P, Rajkumar K C and Madhukar A 1991 *Appl. Phys. Lett.* **58** 1771–3

[31] Park Y, Cich M J, Zhao R, Specht P, Weber E R, Stach E and Nozaki S 2000 *Papers from the 18th North American Conf. on Molecular Beam Epitaxy* vol 18 pp 1566–71

[32] Thornton J M C, Woolf D A and Weightman P 1997 *Surf. Sci.* **380** 548–55

[33] Thornton J M C, Woolf D A and Weightman P 1998 *Appl. Surf. Sci.* **123/124** 115–9

[34] Yang K and Schowalter L J 1992 *Appl. Phys. Lett.* **60** 1851–3

[35] Ratsch C and Venables J A 2003 *J. Vac. Sci. Technol.* A **21** 596–609

[36] Blum V, Gehrke R, Hanke F, Havu P, Havu V, Ren X, Reuter K and Scheffler M 2009 *Comput. Phys. Commun.* **180** 2175–96

[37] Perdew J P, Burke K and Ernzerhof M 1996 *Phys. Rev. Lett.* **77** 3865–8

[38] Wever J, Meyerheim H L, Moritz W, Jahns V, Wolf D, Schulz H, Seehofer L and Johnson R L 1994 *Surf. Sci.* **321** L225–32

[39] Koga H 2010 *Phys. Rev.* B **82** 113301

[40] Biegelsen D K, Bringans R D, Northrup J E and Swartz L E 1990 *Phys. Rev. Lett.* **65** 452–5

[41] Pashley M D 1989 *Phys. Rev.* B **40** 10481–7